Modified Brewster angle on conducting 2D materials

Majerus, Bruno; Cormann, Mirko; Reckinger, Nicolas; Paillet, Matthieu; Henrard, Luc; Lambin, Philippe; Lobet, Michael

Published in:
2D Materials

DOI:
10.1088/2053-1583/aaa574

Publication date:
2018

Document Version
Peer reviewed version

Modified Brewster angle on conducting 2D materials

Bruno Majérus[a,*], Mirko Cormann[a,*], Nicolas Reckinger[a,*], Matthieu Paillet[b], Luc Henrard[a], Philippe Lambin[a], Michaël Lobet[a,c,*]

a Department of Physics & Research Group on Carbon Nanostructures (CARBONNAGe), University of Namur, 61 rue de Bruxelles, 5000 Namur, Belgium
b Laboratoire Charles Coulomb (L2C), Univ. Montpellier, CNRS, Montpellier, France
c John A. Paulson School of Engineering and Applied Sciences, Harvard University, 9 Oxford Street, Cambridge, MA 02138, United States of America
* Those authors contributed equally to the work.

E-mail: luc.henrard@unamur.be

Abstract.

Insertion of 2D materials in optical systems modifies their electrodynamical response. In particular, the Brewster angle undergoes an up-shift if a substrate is covered with a conducting 2D material. This work theoretically and experimentally investigates this effect related to the 2D induced current at the interface. The shift is predicted for all conducting 2D materials and tunability with respect to the Fermi level of graphene is evidenced. Analytical approximations for high and low 2D conductivities are proposed and avoid cumbersome numerical analysis of experimental data. Experimental demonstration using spectroscopic ellipsometry has been performed in UV to NIR range on mono-, bi- and trilayer graphene samples. The non-contact measurement of this modified Brewster angle allows to deduce the optical conductivity of 2D materials. Applications to telecommunication technologies can be considered thanks to the tunability of the shift at $1.55\,\mu m$.

1. Introduction

Two-dimensional (2D) materials are atomically thin structures that often stack into layered solids with strong covalent in-plane bonds and weak van der Waals (vdW) out-of-plane bonds. For the last decade, they are at the forefront of a revolution in material science [1]. This high expectation takes its roots in the quantum confinement of the electrons in the in-plane directions. Furthermore, the absence of surface dangling bonds makes these 2D materials extremely appealing for the realization of vdW heterostructures [2, 3, 4]. Indeed, the lattice mismatch is no longer an issue for the stacking of different crystalline layers interacting via vdW forces.

Despite their vanishing thicknesses, some 2D materials interact strongly with light as exemplified by a single graphene layer, which is able to absorb 2.3% of incoming visible light [5] and 10 times more in the microwave range [6, 7, 8]. Moreover, 2D materials present a rich diversity of electronic structures. Graphene is a semi-metal with ultra high carrier mobility and presents a cone-shaped band structure around the K point [9, 10]. Silicene, germanene, stanene, regrouped inside the 2D-Xenes monoelemental class of 2D crystals, possess electronic structures ranging from insulators to semiconductors to semi-metals [11]. These properties can be modified by strain, chemical functionalization or the interaction with the substrate they are lying on. Other 2D materials like transition metal dichalcogenides (TMDs) and MXenes are shown to have metallic or semiconducting properties [12, 13, 14, 15]. In addition, it should be noted that an interesting feature of most 2D materials is the possibility to modulate their electronic and optical properties by applying an external gate voltage [16]. This huge diversity in electronic and consequently optical properties calls for an efficient and simple determination of the optical 2D conductivity of those materials on a broad range of the electromagnetic (EM) spectrum [17, 18].

Combined with their high flexibility [19], those emerging materials are promising candidates for the realization of nanophotonic devices and to explore fundamental optical effects occurring in low dimensionality devices. Among them, inhibition of p-polarized reflected light at the Brewster angle should be revisited if a conducting 2D material is laid over the surface of a dielectric medium. This phenomenon is technologically important and is used in Brewster windows for gas lasers, for photography or for polarized sunglasses. The modification of this effect due to a conducting 2D material has been theoretically evidenced several times but was never fully investigated to our best knowledge. For example, imaging graphene with p-polarized light at Brewster angle increases its optical contrast [20]. The absorption in monolayer graphene on top of a single-layer guided mode resonant Brewster filter is theoretically supposed to reach 60% [21] and tunable polarization beam splitters were recently conceived theoretically using graphene ribbons [22]. In the latter article, a small shift in the Brewster angle on a graphene ribbon array compared to the one of a simple dielectric film is observed. The deviation of the Brewster angle due to the 2D film is also theoretically mentioned in [23, 24]. An all-dielectric metasurface made of Si nanodisks theoretically and experimentally demonstrated a generalized Brewster effect for arbitrary angle, nanodisk geometry or polarization [25].

In this work, the generalized p-polarized Fresnel coefficient for electromagnetic radiation impinging a conducting 2D material lying on a semi-infinite dielectric substrate is derived. The modification of the Brewster angle is evidenced, microscopically explained and simple and useful analytical approximations are provided. In the terahertz range, this shift is proved to be tunable with respect to the Fermi level. Furthermore, evidence of the shift is demonstrated experimentally for one, two and three graphene

layers. The determination of the Brewster angle provides a non-contact method to determine the effective 2D conductivity of 2D layers or heterostructures. Here, the universal conductivity of graphene in the visible range is retrieved as a proof of principle of this new non-contact method. To the best of our knowledge, this is the first experimental evidence of this phenomenon occurring in 2D materials.

2. Brewster angle for a conducting 2D material

2.1. Microscopic interpretation of the Brewster angle

The Brewster effect occurs when light is not reflected in p-polarization (figure 1(a)) [26]. This arises when the polarization density $\boldsymbol{P}_{tot}$ in the dielectric material is parallel to the wavevector of the reflected wave $\boldsymbol{k_r}$. In this case, the only component of the polarization density is due to the local electric dipoles excited by the refracted wave, i.e. $\boldsymbol{P}_{tot} = \boldsymbol{P}_{bulk}$. It follows that $\theta_B + \theta_{B2} = \pi/2$ where θ_B stands for the incident Brewster angle and θ_{B2} for the corresponding refracted angle. The well-known formula is retrieved from Snell law:

$$\tan\theta_B = \frac{n_2}{n_1}. \tag{1}$$

This situation is no longer valid once a conducting 2D material lies at the interface (figure 1 (b)). Indeed, a planar current density, $\boldsymbol{J}_{2D} = \sigma_{2D}\boldsymbol{E}$ with σ_{2D} the 2D conductivity, can occur and is related to a planar component of the polarization density $\boldsymbol{P}_{2D}$. The higher the 2D conductivity, the closer to the interface the total polarization density direction and the higher the Brewster angle shift. In the limit of an infinite 2D conductivity, the modified Brewster angle θ'_B tends to $\pi/2$.

2.2. Modified Brewster angle

To calculate the modified Brewster angle, the generalized reflection Fresnel coefficient in p-polarization should be canceled out once a 2D conducting plane is inserted between two semi-infinite dielectric media. Assuming that the 2D conducting layer is not charged, one obtains the reflectance [27, 28, 29]:

$$R_p = \left| \frac{n_1\cos\theta_2 - n_2\cos\theta_1 - \frac{\sigma_{2D}}{\epsilon_0 c}\cos\theta_1\cos\theta_2}{n_1\cos\theta_2 + n_2\cos\theta_1 + \frac{\sigma_{2D}}{\epsilon_0 c}\cos\theta_1\cos\theta_2} \right|^2. \tag{2}$$

To obtain the exact value of this modified Brewster angle θ'_B for real σ_{2D}, one should cancel R_P, i.e,

$$\frac{\sigma_{2D}}{\varepsilon_0 c} = \frac{n_1}{\cos\theta'_B} - \frac{n_2}{\cos\theta'_{B2}}. \tag{3}$$

This equation can be solved numerically to extract θ'_B for a given σ_{2D}. For example, CVD graphene in the microwave range has a 2D conductivity $\sigma_{2D} = 0.37\,\varepsilon_0 c$ (at $30\,GHz$, see next section). As shown in figure 2(a), the subsequent shift of the Brewster angle

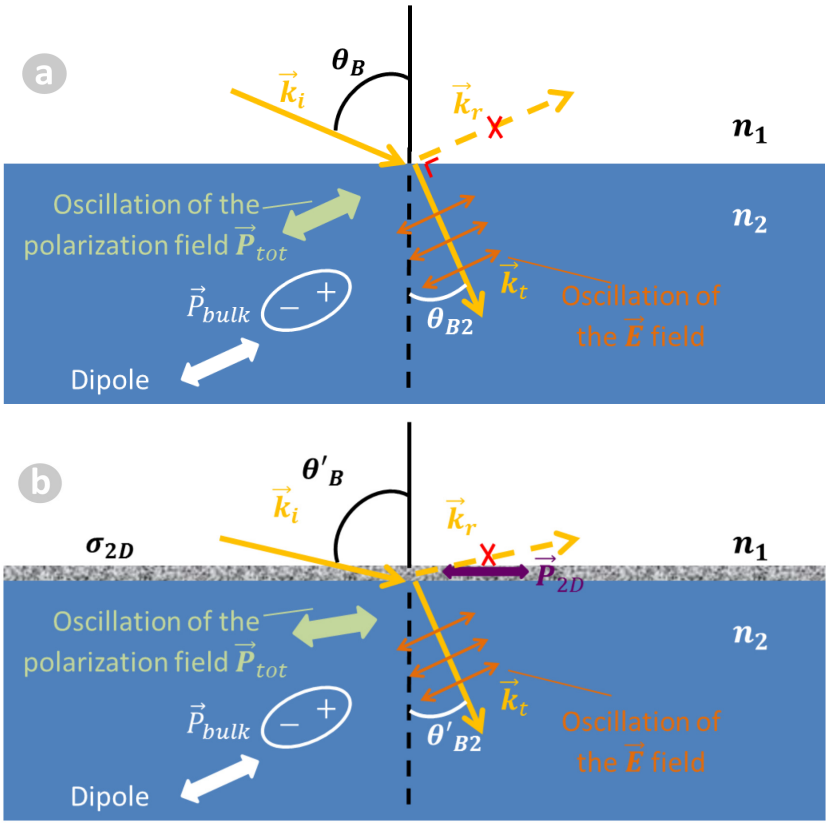

Figure 1. Incident p-polarized electromagnetic wave of wavevector $\boldsymbol{k_i}$ at incident Brewster angle θ_B impinging on the interface between two dielectric media of refractive indexes n_1 and n_2. The reflected (transmitted) wave has a wave vector $\boldsymbol{k_r}$ ($\boldsymbol{k_t}$) and the reflected (refracted) angle θ_B (θ_{B2}) (a) Classical Brewster effect, (b) Modified Brewster effect due to the presence of a 2D conducting layer at the interface.

is 4.6° ($n_1 = 1$, $n_2 = 1.92$). If the imaginary part of the conductivity is non-zero, the minimum reflectance in p-polarized radiation is never nullify and yields its minimal value (R_0) at the quasi-Brewster angle θ_{QB}. However, even for an intentionally high imaginary part (for instance $\Re(\sigma) = \Im(\sigma)$), modifications are minor, i.e. R_0 is very small and $\theta_{QB} \approx \theta'_B$ (figure 2 (a)).

Equation (3) can be solved approximately if the refractive index of the substrate is higher than the refractive index of the incident medium ($n_2 > n_1$). Depending on whether the conductivity is relatively high or low, the shift of the Brewster angle $\Delta = \theta'_B - \theta_B$, can be expressed as follow (a detailed derivation is provided in supplementary information (SI) (1)):

$$\Delta_{high\,\sigma} \simeq \arctan\left(\frac{n_1 \frac{\sigma_{2D}}{\varepsilon_0 c}}{n_2\sqrt{n_1^2+n_2^2}+n_2\frac{\sigma_{2D}}{\varepsilon_0 c}}\right), \tag{4}$$

$$\Delta_{low\,\sigma} \simeq \frac{n_1(\,\sigma_{2D}/\varepsilon_0 c)}{n_2^2}. \tag{5}$$

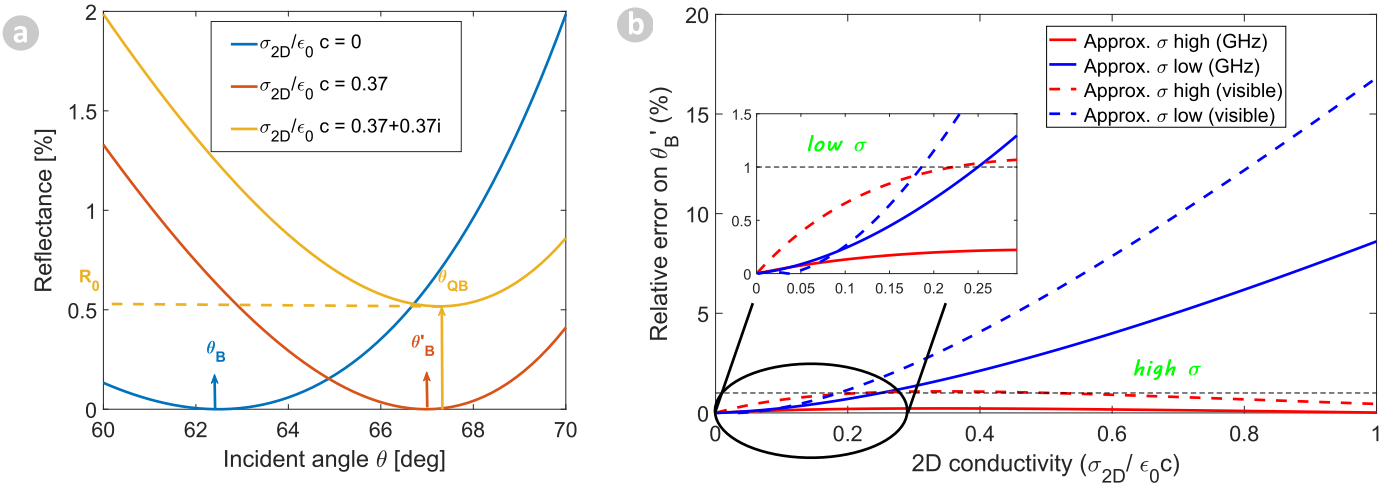

Figure 2. (a) Reflectance in p-polarized radiation of a single graphene layer lying over a silicate substrate ($n_2 = 1.92$) at $30\,GHz$ for the bare substrate (blue line), a real conductivity ($\sigma_{2D} = 0.37$, red line) and a conductivity with an artificially high imaginary part ($\sigma_{2D} = 0.37 + 0.37i$, yellow line). The Brewster angle θ_B of bare substrate, the modified Brewster angle θ'_B due to the presence of a 2D conductivity at the interface and the modified quasi-Brewster angle θ_{QB} are indicated on the figure. (b) Relative errors on the different approximations for the visible range ($n_2 = 1.5$, dotted line) and the GHz range ($n_2 = 1.92$, full line).

The first expression can be equivalently written as:

$$\tan\theta'_B \simeq \frac{n_2 + \frac{\sigma_{2D}}{\varepsilon_0 c} / \sin\theta_B}{n_1} = \frac{n_{2,eff}}{n_1} \tag{6}$$

which defines, by identification with equation (1), the effective refractive index $n_{2,eff}$ of the substrate coated with a 2D material.

Figure 2 (b) depicts the relative error made on θ'_B, compared with the full numerical solution (eq. 3) as a function of the 2D conductivity if one uses the first approximation, equation (4) (red lines, high σ) or the second approximation, equation (5) (blue lines, low σ). The horizontal dashed line indicates a 1% error and defines our domain of validity of the approximations. Two cases were considered since the approximations are dependent on the refractive index of the substrate i.e. $n_2 = 1.92$ (solid lines, silica glass in the GHz range) and $n_2 = 1.5$ (dashed lines, silica glass in the visible range). It should be emphasized that those approximations were derived considering the 2D conductivity to be purely real. However, as demonstrated earlier, θ_{QB} and $\theta_{B'}$ do not significantly differ for a small imaginary part of the 2D conductivity. In summary, for each particular case, it is always possible to choose an approximation leading to an relative error smaller than 1%.

2.3. Application to graphene and other 2D materials

The most popular conducting 2D material is graphene. Its conductivity at $30\,GHz$ has been evaluated to $\sigma_{2D} = 0.37\,\varepsilon_0 c$ i.e. $9.8 \times 10^{-4}\,S/m$, corresponding to a relaxation time

of $75fs$ and a doping carrier density $n = 9.1 \times 10^{15}\, e/m^2$ [28]. In the visible, the 2D conductivity is defined by the universal constant $\sigma_0 = \frac{e^2}{4\hbar} = \pi\alpha\varepsilon_0 c = 0.023\,\varepsilon_0 c$. Those two cases correspond respectively to the high and low conductivities cases defined in the previous section. For a complete description of the graphene optical conductivity, one can use the Kubo formula [17, 27, 31, 32] with corrections to account for excitonic effects near the saddle-point singularity in graphene band structure (see SI (2) for more details). Temperature here is $T = 300\,K$, while the relaxation time is fixed as previously, $\tau = 75\,fs$. The hopping parameter from the tight-biding model is $t = 2.6\,eV$ and the parameters of the Fano model for the excitonic correction are $q = -1.4\,eV$, $E_{res} = 4.85\,eV$, $\Gamma = 780\,meV$ [17]. The Brewster angle can be tuned by adjusting the Fermi level E_F as depicted in figure 3 for different realistic values of the Fermi level and for a single layer of graphene deposited on silica glass with a frequency dependent refractive index reported in the literature [33]. The modification of the Fermi level from 0.3 to $0.5\,eV$ causes a shift as high as $\Delta \approx 1°$ in the C-band (around $1550\,nm$) of telecommunications. The largest shift in Brewster angle is predicted around $266\,nm$ related to the excitonic resonance [17, 32].

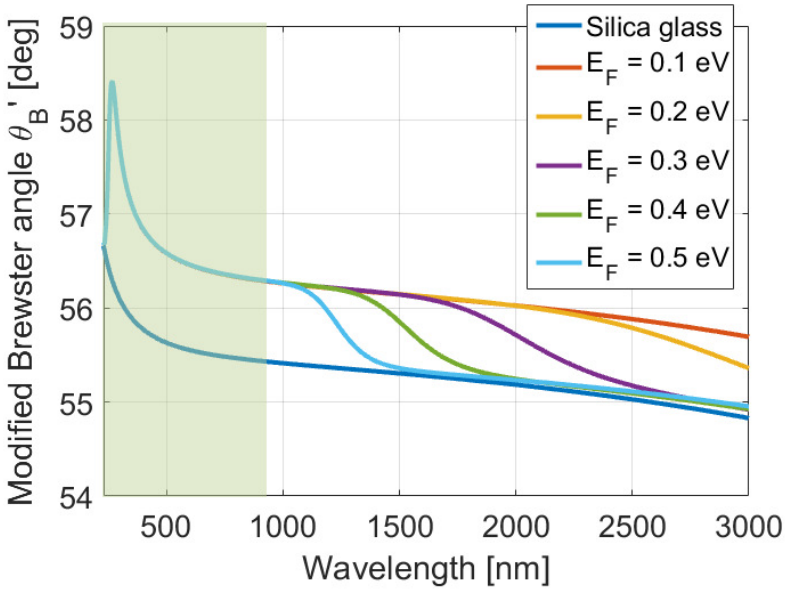

Figure 3. Modified Brewster angle for graphene deposited on silica glass for several Fermi level obtained by solving equation (3) numerically. The shaded area corresponds to the region of the experiment, i.e. UV, visible and near-infrared.

Other conducting 2D materials are emerging such as silicene, germanene or stanene. Optical conductivities of those materials are scarcely available [34, 35]. Table 1 reports the expected shift in Brewster angle at some particular wavelengths using data from [34]. The substrate is considered as silica glass [33]. The shift can also be quite large for those other 2D materials even in the visible range.

$2D\,material$	$\sigma/\varepsilon_0 c$	$Wavelength\,\lambda\,[nm]$	$\Delta\theta\,[deg]$
Stanene	0.092	708	2.5
Stanene	0.177	413	4.7
Stanene	0.1898	331	5.0
Silicene	0.093	608	2.5
Silicene	0.328	260	8.3
Germanene	0.092	608	2.5
Germanene	0.188	342	5.0
Germanene	0.171	273	4.4

Table 1. Shift in Brewster angle due to a conducting 2D material deposited on silica glass for several wavelengths. The 2D conductivity is taken form reference [34] and the shift is calculated using equation (5).

Heterostructures and multilayers of 2D materials can also be considered in order to modify the conductivity. If the total thickness of the vdW heterostructure is smaller than the average skin depth, the effective 2D conductivity can be defined as the sum of the conductivity of each 2D material layer i.e. $\sigma_{2D,tot} = \sum \sigma_{2D,i}$ [6, 17]. This approximation stands if the different layers are electronically decoupled with respect to each other, e.g. by the insertion of a dielectric layer or by a stacking twist in the case of graphene.

Finite substrate thickness modifies the Brewster angle because of the internal reflexion at the second interface. A detail derivation is presented in SI (3) and it is shown that, if the substrate thickness is larger than the coherence length of light (typically of the order of the hundred of micrometers for visible light), Δ is reduce to half the value evaluate for semi-infinite substrates.

In this section, a tunable shift in the Brewster angle has been numerically evidenced and relations between the shift and the 2D conductivity analytically given. In the next section this outcome will be verified experimentally and used to determine the conductivity of a graphene multilayer from non-contact optical measurement.

3. Experimental methods

3.1. Fabrication of the samples

Samples with respectively one, two and three graphene layers transferred on silica glass were fabricated (figure 4(a)). The monolayer graphene films were synthesized by atmospheric pressure chemical vapor deposition on commercial copper foils (Alfa Aesar, 25-μm-thick, 99.8% purity). The copper pieces ($1 \times 2\,cm^2$) were first cleaned by ultrasonication in a mixture of acetic acid and deionized (DI) water, rinsed in DI water, and blow-dried with nitrogen. The growth was performed in a hotwall furnace, in the presence of dilute methane ($0.5\,sccm$ of a mixture of argon and methane with a 95 : 5

ratio), hydrogen (20 *sccm*), and argon (500 *sccm*) for one hour [36].

The resulting polycristalline (maximal domain size of $20\,\mu m$) graphene films were transferred on a 1 mm-thick silica glass slide (Thermo Scientific microscope slides) with the widespread polymer-assisted technique. More specifically, poly(methyl methacrylate) (PMMA) was first spin-coated on the graphene/copper pieces. Then, after removing graphene grown on the backside of the copper substrates by oxygen plasma, the PMMA/graphene/copper stacks were floated on ammonium persulfate until complete copper etching (within a few hours). Next, the PMMA/graphene films were rinsed with DI water and fished onto the glass slide. Finally, after drying overnight in air, the samples were baked on a heating plate at $120\,^{\circ}C$ to improve graphene adhesion on glass and PMMA was removed by soaking in acetone. The same process was repeated three times successively, by appropriately shifting the three transferred monolayer sheets relatively to each other to produce mono-, bi-, and trilayer graphene areas on the same slide.

These growing conditions are known to lead to uniform polycristalline graphene layers. The transfer process lead to randomly oriented graphene layer.

3.2. Raman spectroscopy and optical contrast characterization

The samples were then characterized by simultaneous micro-reflection and micro-Raman mapping using a home-made set-up as described in [37, 38] and detailed in the SI (4). In order to obtain statistical information on the number of graphene layers on each region investigated by ellipsometry, the approach detailed in [38] is followed. In brief, first, the A_G^{norm} and the laser optical contrast (OC) are extracted from the recorded maps. A_G^{norm} is the integrated G-band intensity normalized to the one of highly oriented pyrolytic graphite. The laser OC is defined by $(R_s - R)/R_s$, where R (respectively R_s) is the reflected intensity of the $532\,nm$ laser light measured on each point of the sample (respectively on the bare substrate). The map consist of more than 20000 measurements for each area Then, expressions from [38] are used to calculate the numbers of layers N_G (respectively N_{OC}) estimated from A_G^{norm} (respectively OC). On Figure 4(b), the 3D bivariate histograms of N_G and N_{OC} as well as the histograms for each independent quantities are displayed for each measured regions. As detailed in Ref. [38], both criteria (A_G^{norm} and OC) can fail to determine the correct number of layers due to specific responses related to the relative orientation of the graphene layers but also to the present of residues, contaminations and/or defects. In other words, the values of N_G and N_{OC} have to be in agreement according to the criteria defined in [38] to ensure the reliability of the estimated number of layers by this method. The number of layers is attributed when the data are found to fall within specific ranges as illustrated in Figure 4(b). Other points are set as non-attributed (NA). The number of layers histograms obtained using such analysis are shown in Figure 4(c) and clearly confirm that the first region is mainly composed of one layer graphene, the second of two layers graphene and the third of three layers graphene. Before to go further in the estimation of the number

of layers distributions, one should notice that the proportions of NA points are 20% for the one layer region, 55% for the two layers region and 65% for the three layers region. Further analysis of the data (not shown) enable us to infer that, for all three regions, the amount of impurities (transfer residues, dusts, holes, defects...) represents about 20% of the data, i.e. almost the totality of NA points in the one layer region but a minority of them for the two layers and three layers regions. The remaining NA points in these two regions are related to optical resonance effects arising for some relative twist angle between consecutive layers [38]. The OC is much less influenced by such optical resonances especially when the graphene layers are deposited on glass as it is the case here. The similarities between the N_{OC} histograms and the number of layers histograms clearly show that the obtained distributions are not significantly distorted by the exclusion of NA points. To summarize, it is estimated that all three regions are 80% clean and the clean parts compositions obtained are: 1) $> 95\%$ of one layer for the one layer region, 2) $> 85\%$ of two layers, 5% of one layer and 5% of three layers for the two layers region and 3) $> 65\%$ of three layers, $10 - 15\%$ of two layers and $5 - 15\%$ of four layers for the three layers region. The average number of layers for each region thus fits very well with the targeted one. The lower than expected amount of three layers in the three layers region is mainly due to a partial ripping and folding of one of the transferred layer as observed by optical microscopy (not shown).

3.3. Ellipsometry measurements

The determination of the modified Brewster angle rests on spectroscopic ellipsometry (Sopra GES-5E) from the ultraviolet (UV) to the near-infrared (NIR) spectral range, i.e. from 230 to $960\,nm$. The 2D materials are analyzed using photometric rotating polarizer ellipsometry (RPE) at several incident angles θ. The spectral and angular evolution of one of the two normalized Fourier coefficients of the ellipsometric signal (the β coefficient) [39], is used to determine the Brewster angles. At a given wavelength, the coefficient β is acquired for several incident angles around the Brewster angle of the glass substrate, here from 52° to 64° by step of 0.2°. Close to the Brewster angle, β depends linearly on the incident angle θ and its value is zero at this particular angle [39]. The Brewster angle is deduced by fitting the data using a linear regression model.

4. Results and Discussions

The value of the Brewster angle shift Δ can be evaluate for a single graphene layer in the NIR-visible domain if one uses the universal conductivity ($\sigma_0 = \pi\alpha\,\varepsilon_0 c$) in equation (5) divided by two to take backside reflections into accounts. With $n_1 = 1$ and $n_2 = 1.5$, one gets

$$\Delta \approx \frac{1}{2}\frac{n_1}{n_2^2}\pi\alpha \approx 0.29°. \tag{7}$$

Figure 5 (a) shows the experimental Brewster angle measured on the bare glass

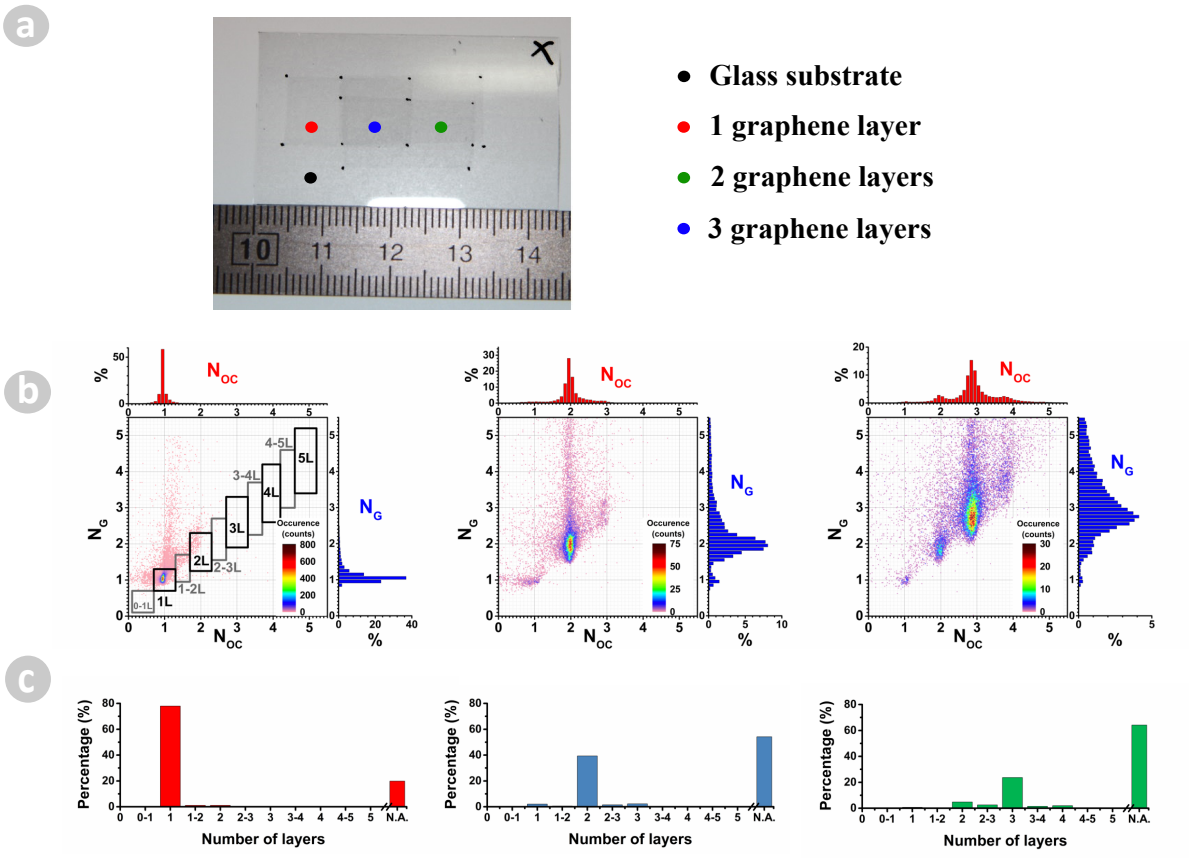

Figure 4. (a) Optical image of the multilayer sample. (b) 3D bivariate histogram (0.025 bin size) of N_{OC} and N_G (see text) for the one layer region (left), the two layers region (middle) and the three layers region (right). The number of occurrences (frequency counts) is color coded as shown on the graphs. On top (respectively right hand side) are displayed the corresponding histograms of N_OC (respectively N_G). In (a) - left panel, the black and grey squares correspond to the integration ranges used to obtain the number of layers histograms (c). The black regions correspond each to a given number of layers while the grey regions correspond to non-integer numbers of layers as shown on the graph. The points out of these regions are considered as non-attributed (NA). (c) Number of layers histograms for the one layer region (left), the two layers region (middle) and the three layers region (right) extracted from (b).

substrate, as well as on mono-, bi- and trilayer graphene areas. The figure represents the mean values of the Brewster angle with the corresponding confidence interval (confidence level arbitrarily fixed at 99.9%), resulting from data analysis on 9 different acquisitions on arbitrarily selected zones of each graphene area. An increase of the Brewster angle of about 0.3° per graphene layer is observed in the visible range, in very good agreement with the prediction (eq. 7). In the UV spectral range, the peaks at 268 nm correspond to the two-dimensional saddle-point exciton. This confirms that the deposited graphene causes these modifications of the Brewster angle [18].

The optical conductivity of one, two and three layers are deduced from equation (5) (figure 5 (b)). In the visible and near infrared range, the conductivity is close to the

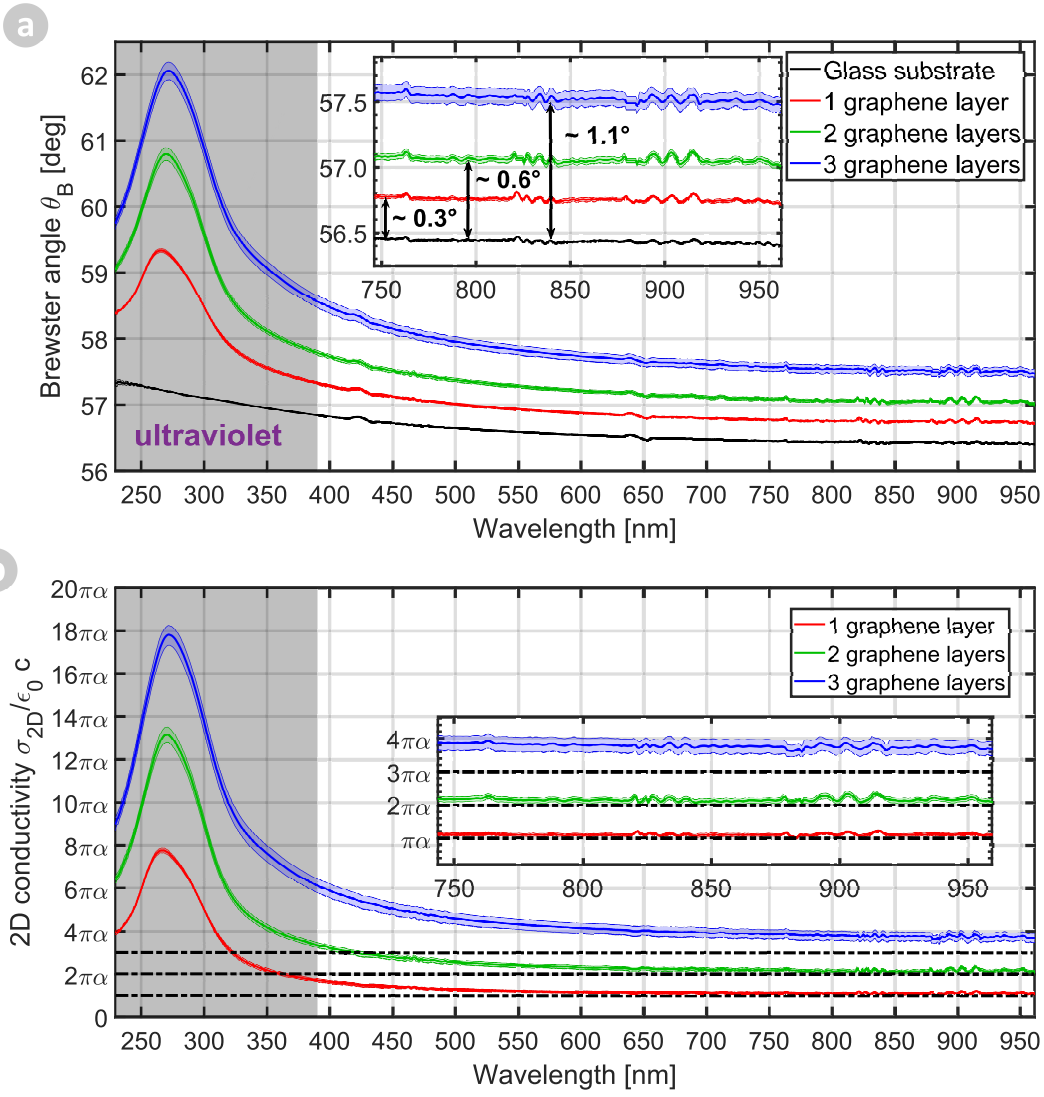

Figure 5. (a) Brewster angle θ_B for a glass substrate (black), a mono- (red), bi- (green) and trilayer (blue) graphene. Inset: zoom in the $750 - 950\,nm$ region. (b) Retrieved conductivity using the second approximation. Doted lines correspond to multiple integers of σ_0.

universal constant value $\sigma_0 = \pi\alpha\,\varepsilon_0 c$ for one layer, and $2\sigma_0$ for two layers, as expected for high quality graphene. The three layer area shows a larger shift than foreseen. This has to be related with the larger uncertainty on the number of layer and the presence of structural imperfection. A detailed investigation of the optical response (Brewster angle modification, optical transmission and reflectance contrast $\Delta R/R$) of multilayer systems correlated with the structural quality of the sample deserve a further study. However, our results are in line with the one obtained by Mak *et al* which are based on the optical measurement of the reflectance contrast [17].

At higher energy (UV), the position of the peak at $268\,nm$ $(4.6\,eV)$ is in good agreement with Mak *et al*. The intensity of the peak is greatly enhanced, nearly

reaching eight times the universal conductivity for a single layer and up to eighteen times for three layers, while the previously cited work gives a maximum value of less than four times the universal conductivity for a single layer and fifteen for three layers. As our approximation of low conductivity is no more valid in this range, we cannot draw quantitative conclusions on the resonant maximal value of the conductivity.

5. Conclusions

A dielectric material coated with 2D materials, display a measurable upshift of the Brewster angle in the UV-visible range compared to the bare substrate. This phenomenon has been explained by the modification of the direction of the polarization density brought about by 2D conducting film at the surface of the substrate. Based on these results, a new non-contact method for the measurement of the optical 2D optical conductivity of 2D materials has been proposed and tested experimentally for the case of graphene. For this purpose, two analytical expressions of the Brewster angle shift for high and low 2D conductivities have been proposed. The validity of the approximation for small conductivity has been verified experimentally and the universal value of the 2D conductivity of graphene has been retrieved. Moreover, the number of layers in multilayer systems can be clearly determined as the 2D conductivity scale linearly with the number of layers. Tunability of this shift with respect to the Fermi level is also discussed, opening opportunities for telecommunication applications.

Acknowledgments

The authors thank Y. Caudano and M. Voué for their insightful remarks related to ellipsometric measurements. This work has been supported by the Belgian Fund for Scientific Research (FRS-FNRS) under FRFC contract. “Chemographene” (convention No 2.4577.11). Part of the research leading to this work received funding from the European Union Seventh Framework Program under grant agreement No 604391 Graphene Flagship and was performed while M. Lobet was a recipient of a Fellowship of the Belgian American Educational Foundation. This research made use of resources of the Electron Microscopy Service at the University of Namur (“Plateforme Technologique Morphologie – Imagerie”). This research has also used computing resources of the "Plateforme Technologique de Calcul Intensif (PTCI)" (http://www.ptci.unamur.be) located at the University of Namur, Belgium, which is supported by the F.R.S.-FNRS under the convention No. 2.4520.11. The PTCI is member of the "Consortium des Equipements de Calcul Intensif (CECI)" (http://www.ceci-hpc.be).

[1] M. S. Dresselhaus. A revolution of nanoscale dimensions. Nature Reviews Materials 1:15017, January 2016.

[2] J. D. Caldwell and K. S. Novoselov. Van der Waals heterostructures: Mid-infrared nanophotonics. Nature Materials, 14(4):364–366, April 2015.

[3] D. Jariwala, T. J. Marks, and M. C. Hersam. Mixed-dimensional van der Waals heterostructures. Nature Materials, 16(2):170–181, February 2017.

[4] A. K. Geim and I. V. Grigorieva. Van der Waals heterostructures. Nature, 499(7459):419–425, July 2013.

[5] R. R. Nair, P. Blake, A. N. Grigorenko, K. S. Novoselov, T. J. Booth, T. Stauber, N. M. R. Peres, and A. K. Geim. Fine Structure Constant Defines Visual Transparency of Graphene. Science, 320(5881):1308–1308, June 2008.

[6] K. Batrakov, P. Kuzhir, S. Maksimenko, A. Paddubskaya, S. Voronovich, P Lambin, T. Kaplas, and Y. Svirko. Flexible transparent graphene/polymer multilayers for efficient electromagnetic field absorption. Scientific Reports, 4:7191, November 2014.

[7] M. Lobet, N. Reckinger, L. Henrard, and P. Lambin. Robust electromagnetic absorption by graphene/polymer heterostructures. Nanotechnology, 26(28):285702, 2015.

[8] K. Batrakov, P. Kuzhir, S. Maksimenko, N. Volynets, S. Voronovich, A. Paddubskaya, G. Valusis, T. Kaplas, Y. Svirko, and P. Lambin. Enhanced microwave-to-terahertz absorption in graphene. Applied Physics Letters, 108(12):123101, March 2016.

[9] A. H. Castro Neto, F. Guinea, N. M. R. Peres, K. S. Novoselov, and A. K. Geim. The electronic properties of graphene. Reviews of Modern Physics, 81(1):109–162, January 2009.

[10] A. C. Ferrari et al. Science and technology roadmap for graphene, related two-dimensional crystals, and hybrid systems. Nanoscale, 7(11):4598–4810, March 2015.

[11] A. Molle, J. Goldberger, M. Houssa, Y. Xu, S.-C. Zhang, and D. Akinwande. Buckled two-dimensional Xene sheets. Nature Materials, 16(2):163–169, February 2017.

[12] B. Anasori, M. R. Lukatskaya, and Y. Gogotsi. 2D metal carbides and nitrides (MXenes) for energy storage. Nature Reviews Materials, 2(2): 16098, January 2017.

[13] H. Weng, A. Ranjbar, Y. Liang, Z. Song, M. Khazaei, S. Yunoki, M. Arai, Y. Kawazoe, Z. Fang, and X. Dai. Large-gap two-dimensional topological insulator in oxygen functionalized MXene. Physical Review B, 92(7):075436, August 2015.

[14] M. Khazaei, A.Ranjbar, M. Arai, and S. Yunoki. Topological insulators in the ordered double transition metals M'2M"C2 MXenes (M'=Mo,W , M"= Ti,Zr,Hf) Physical Review B, 94(12):125152, September 2016.

[15] H. Fashandi, V. Ivády, P. Eklund, A. Lloyd Spetz, M. I. Katsnelson, and I. A. Abrikosov. Dirac points with giant spin-orbit splitting in the electronic structure of two-dimensional transition-metal carbides. Physical Review B, 92(15):155142, October 2015.

[16] F. Wang, Y. Zhang, C. Tian, C. Girit, A. Zettl, M. Crommie, and Y. Ron Shen. Gate-Variable Optical Transitions in Graphene. Science, 320(5873):206–209, April 2008.

[17] K. F. Mak, J. Shan, and T. F. Heinz. Seeing Many-Body Effects in Single- and Few-Layer Graphene: Observation of Two-Dimensional Saddle-Point Excitons. Physical Review Letters, 106(4):046401, January 2011.

[18] V. G. Kravets, A. N. Grigorenko, R. R. Nair, P. Blake, S. Anissimova, K. S. Novoselov, and A. K. Geim. Spectroscopic ellipsometry of graphene and an exciton-shifted van Hove peak in absorption. Physical Review B, 81(15):155413, 2010.

[19] D.Akinwande, N. Petrone, and J. Hone. Two-dimensional flexible nanoelectronics. Nature Communications, 5:5678, December 2014.

[20] P. Romagnoli, H. Rosa, D. Lopez-Cortez, E. Souza, J. Viana-Gomes, W. Margulis, and C. de Matos. Making graphene visible on transparent dielectric substrates: Brewster angle imaging. 2D Materials, 2(3):035017, September 2015.

[21] G. Zheng, H. Zhang, L. Xu, and Y. Liu. Enhanced absorption of graphene monolayer with a single-layer resonant grating at the Brewster angle in the visible range. Optics Letters, 41(10):2274–2277, May 2016.

[22] Y. Tang, Z. Zhu, J. Zhang, C. Guo, X. Yuan, and S. Qin. Electrically tunable graphene polarization beam splitting utilizing Brewster effect. Journal of Optics, 18(2):025002, 2016.

[23] Y. Bludov, N. Peres, and M. Vasilevskiy. Unusual reflection of electromagnetic radiation from a

stack of graphene layers at oblique incidence. Journal of Optics, 15(11):114004, October 2013.

[24] V. Meera and G. S. Setlur. Ellipsometry of graphene on a substrate. Journal of Applied Physics, 107(3):033525, February 2010.

[25] R. Paniagua-Dominguez, Y. F. Yu, A. E. Miroshnichenko, L. A. Krivitsky, Y. H. Fu, V. Valuckas, L. Gonzaga, Y. T. Toh, A. Y. S. Kay, B. L. yanchuk, and A. I. Kuznetsov. Generalized Brewster effect in dielectric metasurfaces. Nature Communications, 7:10362, January 2016.

[26] O. Stenzel. The Physics of Thin Film Optical Spectra - An Introduction | Olaf Stenzel | Springer. 1996.

[27] L. A. Falkovsky. Optical properties of graphene. Journal of Physics: Conference Series, 129(1):012004, 2008.

[28] M. Lobet, N. Reckinger, L. Henrard, and P. Lambin. Robust electromagnetic absorption by graphene/polymer heterostructures. Nanotechnology, 26(28):285702, 2015.

[29] M. Lobet, B. Majerus, L. Henrard, and P. Lambin. Perfect electromagnetic absorption using graphene and epsilon-near-zero metamaterials. Physical Review B, 93(23):235424, 2016.

[30] B. Huttner. On Brewster s angle of metals. Journal of Applied Physics, 78(7), October 1995 4799–4801.

[31] F. J. G. de Abajo. Graphene Plasmonics: Challenges and Opportunities. ACS Photonics, 1(3):135–152, March 2014.

[32] T. Stauber, N. M. R. Peres, and A. K. Geim. Optical conductivity of graphene in the visible region of the spectrum. Physical Review B, 78(8):085432, August 2008.

[33] R. Kitamura, L. Pilon, and M.Jonasz. Optical constants of silica glass from extreme ultraviolet to far infrared at near room temperature. Applied Optics, 46(33):8118–8133, November 2007.

[34] L. Matthes, O. Pulci, and F. Bechstedt. Optical properties of two-dimensional honeycomb crystals graphene, silicene, germanene, and tinene from first principles. New Journal of Physics, 16(10):105007, 2014.

[35] R. John and B. Merlin. Optical properties of graphene, silicene, germanene, and stanene from IR to far UV A first principles study. Journal of Physics and Chemistry of Solids, 110:307–315, November 2017.

[36] N.Reckinger, X. Tang, F. Joucken, L. Lajaunie, R. Arenal, E. Dubois, B. Hackens, L. Henrard, and J.-F. Colomer. Oxidation-assisted graphene heteroepitaxy on copper foil. Nanoscale, 8(44):18751–18759, November 2016.

[37] M. Bayle, N. Reckinger, J.-R. Huntzinger, A. Felten, A. Bakaraki, P. Landois, J.-F. Colomer, L. Henrard, A.-A. Zahab, J.-L. Sauvajol and M. Paillet. Dependence of the Raman spectrum characteristics on the number of layers and stacking orientation in few-layer graphene physica status solidi (b), 252(11), 2375–2379, 2016

[38] M. Bayle, N. Reckinger, A. Felten, P. Landois, O. Lancry, B. Dutertre, J.–F. Colomer, A.-A. Zahab, L. Henrard, J.-L. Sauvajol and M. Paillet. Determining the number of layers in few-layer graphene by combining Raman spectroscopy and optical contrast Journal of Raman Spectroscopy In press 2017

[39] H. Fujiwara. Spectroscopic Ellipsometry: Principles and Applications | Wiley. 2007.